Novel ultra-broadband polarization splitter-rotator based on mode-evolution tapers and a mode-sorting asymmetric Y-junction

Jing Wang,[1,2] Ben Niu,[2] Zhen Sheng,[1] Aimin Wu,[1] Wei Li,[1] Xi Wang,[1] Shichang Zou,[1] Minghao Qi,[2,*] and Fuwan Gan[1]

[1]*State Key Laboratory of Functional Materials for Informatics, Shanghai Institute of Microsystem and Information Technology, Chinese Academy of Sciences, Shanghai 200050, China*

[2]*School of Electrical and Computer Engineering and the Birck Nanotechnology Center, Purdue University, West Lafayette, IN 47907 USA*

[*]*mqi@purdue.edu*

Abstract: A novel silicon-on-insulator (SOI) polarization splitter-rotator is proposed based on mode-evolution tapers and a mode-sorting asymmetric Y-junction. The tapers are designed to adiabatically convert the input TM_0 mode into the TE_1 mode, which will evolve into the TE_0 mode in the wide output arm while the input TE_0 mode excites the TE_0 mode in the narrow arm. The numerical simulation results show that the mode conversion efficiency increases with the lengths of the tapers and the Y-junction for the output waveguide widths in a large range. This proposed device has < 0.4 dB insertion loss with > 12 dB extinction ratio in an ultra-broad wavelength range from 1350 nm to 1750 nm. With such a broad operating bandwidth, this device offers potential applications for polarization diversity operating across every communication bands. Fabrication tolerance analysis is also performed in terms of the device width variation, the slab height variation and the variation of the upper-cladding refractive index.

©2014 Optical Society of America

OCIS codes: (130.3120) Integrated optics devices; (230.7370) Waveguides; (130.5440) Polarization-selective devices.

References and links

1. W. Bogaerts, R. Baets, P. Dumon, V. Wiaux, S. Beckx, D. Taillaert, B. Luyssaert, J. Van Campenhout, P. Bienstman, and D. Van Thourhout, "Nanophotonic waveguides in silicon-on-insulator fabricated with CMOS technology," J. Lightwave Technol. **23**(1), 401–412 (2005).
2. C. Manolatou, S. G. Johnson, S. Fan, P. R. Villeneuve, H. A. Haus, and J. D. Joannopoulos, "High density integrated optics," J. Lightwave Technol. **17**(9), 1682–1692 (1999).
3. M. R. Watts, H. A. Haus, and E. P. Ippen, "Integrated mode-evolution-based polarization splitter," Opt. Lett. **30**(9), 967–969 (2005).
4. J. C. Wirth, J. Wang, B. Niu, Y. Xuan, L. Fan, L. Varghese, D. E. Leaird, M. Qi, and A. Weiner, "Efficient Silicon-on-Insulator Polarization Rotator based on Mode Evolution," in *Conference on Lasers and Electro-Optics*, OSA Technical Digest (online) (Optical Society of America, 2012), JW4A.83.
5. T. Barwicz, M. R. Watts, M. A. Popovic, P. T. Rakich, L. Socci, F. X. Kartner, E. P. Ippen, and H. I. Smith, "Polarization-transparent microphotonic devices in the strong confinement limit," Nat. Photonics **1**(1), 57–60 (2007).
6. L. Liu, Y. Ding, K. Yvind, and J. M. Hvam, "Silicon-on-insulator polarization splitting and rotating device for polarization diversity circuits," Opt. Express **19**(13), 12646–12651 (2011).
7. D. Dai and J. E. Bowers, "Novel concept for ultracompact polarization splitter-rotator based on silicon nanowires," Opt. Express **19**(11), 10940–10949 (2011).
8. Y. Ding, L. Liu, C. Peucheret, and H. Ou, "Fabrication tolerant polarization splitter and rotator based on a tapered directional coupler," Opt. Express **20**(18), 20021–20027 (2012).
9. Y. Fei, L. Zhang, T. Cao, Y. Cao, and S. Chen, "Ultracompact polarization splitter-rotator based on an asymmetric directional coupler," Appl. Opt. **51**(34), 8257–8261 (2012).
10. J. Wang, B. Niu, Z. Sheng, A. Wu, X. Wang, S. Zou, M. Qi, and F. Gan, "Design of a SiO_2 top-cladding and compact polarization splitter-rotator based on a rib directional coupler," Opt. Express **22**(4), 4137–4143 (2014).
11. H. Guan, A. Novack, M. Streshinsky, R. Shi, Q. Fang, A. E. Lim, G. Q. Lo, T. Baehr-Jones, and M. Hochberg, "CMOS-compatible highly efficient polarization splitter and rotator based on a double-etched directional coupler," Opt. Express **22**(3), 2489–2496 (2014).

#206996 - $15.00 USD Received 10 Apr 2014; accepted 15 May 2014; published 29 May 2014
(C) 2014 OSA

12. Y. Ding, H. Ou, and C. Peucheret, "Wideband polarization splitter and rotator with large fabrication tolerance and simple fabrication process," Opt. Lett. **38**(8), 1227–1229 (2013).
13. W. D. Sacher, T. Barwicz, B. J. Taylor, and J. K. Poon, "Polarization rotator-splitters in standard active silicon photonics platforms," Opt. Express **22**(4), 3777–3786 (2014).
14. N. Riesen and J. D. Love, "Design of mode-sorting asymmetric Y-junctions," Appl. Opt. **51**(15), 2778–2783 (2012).
15. J. D. Love and N. Riesen, "Single-, Few-, and Multimode Y-Junctions," J. Lightwave Technol. **30**(3), 304–309 (2012).
16. W. Chen, P. Wang, and J. Yang, "Mode multi/demultiplexer based on cascaded asymmetric Y-junctions," Opt. Express **21**(21), 25113–25119 (2013).
17. J. B. Driscoll, R. R. Grote, B. Souhan, J. I. Dadap, M. Lu, and R. M. Osgood, "Asymmetric Y junctions in silicon waveguides for on-chip mode-division multiplexing," Opt. Lett. **38**(11), 1854–1856 (2013).
18. D. Dai, Y. Tang, and J. E. Bowers, "Mode conversion in tapered submicron silicon ridge optical waveguides," Opt. Express **20**(12), 13425–13439 (2012).

1. Introduction

The silicon-on-insulator (SOI) platform, recently developed for many photonic applications has several advantages over glass-based systems, including small device footprint, low-loss nanowire waveguides, high-speed optical modulators and mature CMOS-compatible fabrication process [1]. However, these SOI devices suffer from strong structural birefringence in waveguides due to the high index-contrast between silicon and SiO_2, leading to a polarization-sensitive performance [2]. Some approaches based on the polarization beam splitters (PBS) [3] and polarization rotators (PR) [4] have been developed recently to achieve polarization diversity [5]. Another efficient and promising polarization-manipulating approach is to use a polarization splitter-rotator (PSR) [6–13], which converts different input polarization modes into the same mode before light passes through functional devices. Compared with the approaches using a PBS cascaded with a PR, the PSR offers potential advantages of simpler structures and lower insertion loss (IL). Various structures have been reported based on asymmetric directional couplers (DCs) [6–11], multimode interference couplers (MMIs) [12] and adiabatic couplers [13]. However, in order to satisfy the phase-matching condition, the DC-based PSRs typically have strict constraints on waveguide widths and coupler lengths, which make the performance sensitive to fabrication imperfections and operating wavelengths. Although a linearly tapered DC has been implemented to relax the requirements on these device sizes, the coupling efficiency is significantly decreased [8]. Another fabrication-tolerant MMI-based PSR with a large bandwidth has been reported recently [12], but this device has complex structures, including a mode-evolution taper, a Y-junction, a phase shifter and a MMI. Very recently, a mode-evolution PSR has been demonstrated in standard silicon photonic platforms, but the coupler length is relatively large [13].

Symmetric Y-junctions, which function as a standard structure in the integrated optics, are well-known as power splitters and often used in the Mach-Zehnder interferometers and optical modulators. However, another type of Y-junctions [14,15], which have two asymmetric output arms, has received much less attention. For an asymmetric Y-junction with a small angle between the output arms, the input mode in the stem will propagate through the Y-junction and adiabatically evolve into the mode in the arm, which has the closest effective refractive index with that of the input mode. By appropriately choosing the arm widths, different modes in the stem will excite the mode in different arms. Previous implementations of asymmetric Y-junctions were focusing on the on-chip mode-division multiplexing (MDM) [16,17] and it is similarly interesting to incorporate this structure into polarization diversity scheme.

In this work, we propose a novel ultra-broadband PSR design based on two basic broadband mode-evolution structures (a mode-evolution taper and a mode-sorting asymmetric Y-junction) in SOI platforms. By optimizing the length of each section of the tapers, high mode conversion efficiency from the TM_0 mode to the TE_1 mode is achieved. Unlike the DC-based PSR which requires a strict phase-matching condition on the waveguide widths and the corresponding coupler lengths, the output arm widths in our device can be chosen in a large range with high mode conversion efficiency as long as the Y-junction length is large enough.

#206996 - $15.00 USD Received 10 Apr 2014; accepted 15 May 2014; published 29 May 2014
(C) 2014 OSA

Therefore, our device offers a significantly improved operating bandwidth compared to all the existing PSR devices to the best of our knowledge. The simulation results shows that a low IL of < 0.4 dB with > 12 dB extinction ratio (ER) is achieved in a broad wavelength range over 400 nm when the device length is 95 μm. Moreover, the performance degradation caused by the imperfect fabrication is analyzed, showing that our device has a large fabrication tolerance.

2. Device design

Figure 1(a) schematically shows the proposed PSR structures, which consists of a taper and an asymmetric Y-junction. This device is designed in SOI rib waveguides with 250 nm rib height, 50 nm slab height and SiO_2 upper-cladding, which is used to break the symmetry in the waveguide cross-section as well as to protect the device. On one hand, the input fundamental transverse-magnetic mode (TM_0) will be converted into the first-order transverse-electric mode (TE_1) in the taper due to the mode coupling in these two modes [18]. Then the TE_1 mode will evolve into the fundamental transverse-electric mode (TE_0) in the narrow output arm (port 2) of the Y-junction because these two modes have the closely matched effective index. On the other hand, the input TE_0 mode is not converted into any other guided mode in the taper and will excite the TE_0 mode in the wide arm (port 1) if the waveguide width is appropriately chosen.

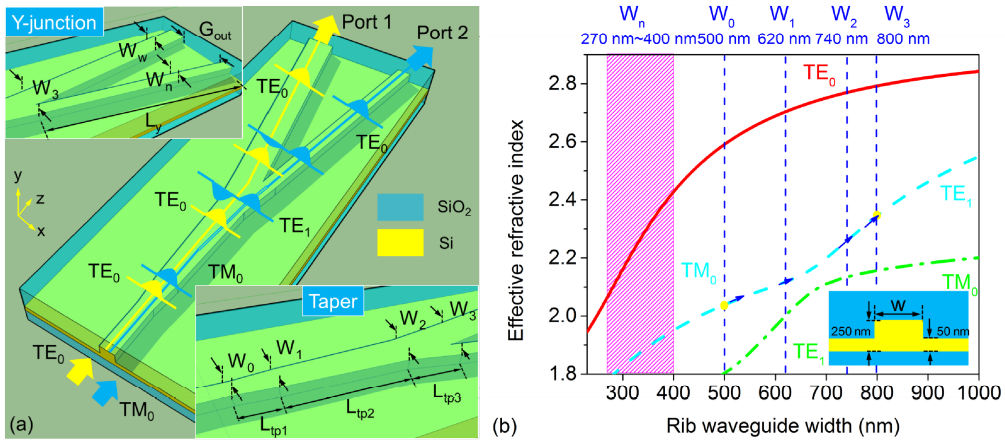

Fig. 1. (a) Schematic of the proposed PSR consisting of mode-evolution tapers and a mode-sorting asymmetric Y-junction. (b) Effective indices of the first three modes in a rib waveguide as a function of the waveguide width. The rib waveguide has a 250 nm rib height and 50 nm slab height. The wavelength is 1550 nm in the simulation.

First, we used a commercial simulation software package (FIMMWAVE) to calculate the effective indices of the first three modes in an SOI rib waveguide, as shown in Fig. 1(b). The refractive indices of Si and SiO_2 are chosen to be $n_{Si} = 3.476$ and $n_{SiO2} = 1.528$, respectively. It can be seen that there is a mode hybridization region for the TM_0 mode and the TE_1 mode when the waveguide width varies from $W_1 = 620$ nm to $W_2 = 740$ nm. Therefore, in order to convert the input TM_0 mode into the TE_1 mode and simultaneously avoid the mode hybridization at the ends of the taper [7], the taper comprises three sections with linearly tapered widths ranging from $W_0 = 500$ nm to $W_1 = 620$ nm, $W_1 = 620$ nm to $W_2 = 740$ nm and $W_2 = 740$ nm to $W_3 = 800$ nm, respectively. The widths of the arms in the asymmetric Y-junction satisfy the relationship as $W_n + W_w = W_3$, where W_n and W_w are the widths of the narrow and wide output arms, respectively. One can note that W_n can be chosen from 270 nm to 400 nm based on the mode-sorting principle of the asymmetric Y-junction. The minimum of W_n is determined by the fact that when $W_n < 270$ nm (corresponding to $W_w > 530$ nm), $|Neff_{W3,TE1} - Neff_{Ww,TM0}| < |Neff_{W3,TE1} - Neff_{Wn,TE0}|$, where $Neff_{w,\ mode}$ denotes the effective refractive index of the *mode* when the waveguide width is *w*. It means the TE_1 mode in the

#206996 - $15.00 USD Received 10 Apr 2014; accepted 15 May 2014; published 29 May 2014
(C) 2014 OSA

stem will evolve into the TM_0 mode in the wide arm instead of the TE_0 mode in the narrow arm, leading to an incorrect mode-sorting.

A three-dimensional simulation software package (FIMMPROP) based on eigen-mode expansion (EME) method was used to optimize the mode conversion efficiency in the taper. Figure 2 shows that the mode conversion efficiency from the TM_0 mode into the TE_1 mode is very close to 1 at appropriately chosen L_{tp2} for a given L_{tp1}. In addition, a larger L_{tp1} will lead to smaller ripples in the conversion curves, which means a larger fabrication tolerance. Here we choose L_{tp1} = 10 μm and L_{tp2} = 50 μm to realize a high efficiency mode conversion in a broadband wavelength range. The mode propagation in the taper for the TE_0 mode and the TM_0 mode at the 1550 nm wavelength with the optimal sizes are shown in the insets of Fig. 2.

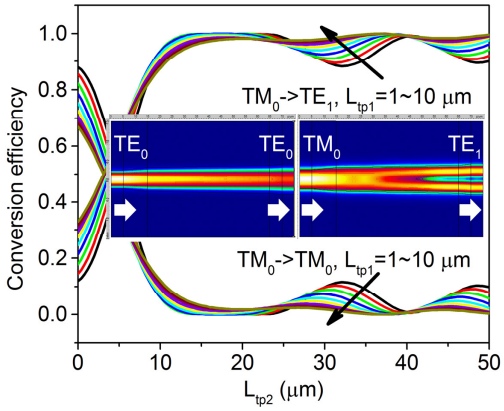

Fig. 2. The mode conversion efficiency for the input TM_0 mode as a function of L_{tp2} for L_{tp1} varying from 1 μm (black) to 10 μm (dark yellow), where L_{tp3} is set to $L_{tp1}(W_3-W_2)/(W_1-W_0)$. Insets: the mode propagation for TE_0 and TM_0 modes in the taper at the 1550 nm wavelength when L_{tp1} = 10 μm, L_{tp2} = 50 μm and L_{tp3} = 5 μm.

The simulated mode conversion efficiency in the Y-junction as a function of the Y-junction length L_y at the 1550 nm wavelength is shown in Fig. 3. The modes (TE_1 and TE_0) launched into the stem will evolve into the specific mode in the output arms. The final gap between the output ports is G_{out} = 1 μm. When W_n varies in a large range from 284 nm to 374 nm, high mode conversion efficiency with correct mode-sorting can be achieved for different input modes and the conversion efficiency increases with the length L_y of the Y-junction as shown in Figs. 3(a) and 3(b). However, some ripples can be seen in Fig. 3(c) when W_n = 274 nm because $|Neff_{W3,TE1} - Neff_{Ww,TM0}|$ is very close to $|Neff_{W3,TE1} - Neff_{Wn,TE0}|$ in this case, leading to a undesirable mode coupling. Nevertheless, the correct mode-sorting with high mode conversion efficiency still occurs when the length is large enough. Figure 3(d) shows an incorrect mode-sorting in the Y-junction, where the input TE_1 mode will evolve into the TM_0 mode in port 1, which should be avoided when choosing the waveguide widths.

#206996 - $15.00 USD Received 10 Apr 2014; accepted 15 May 2014; published 29 May 2014
(C) 2014 OSA

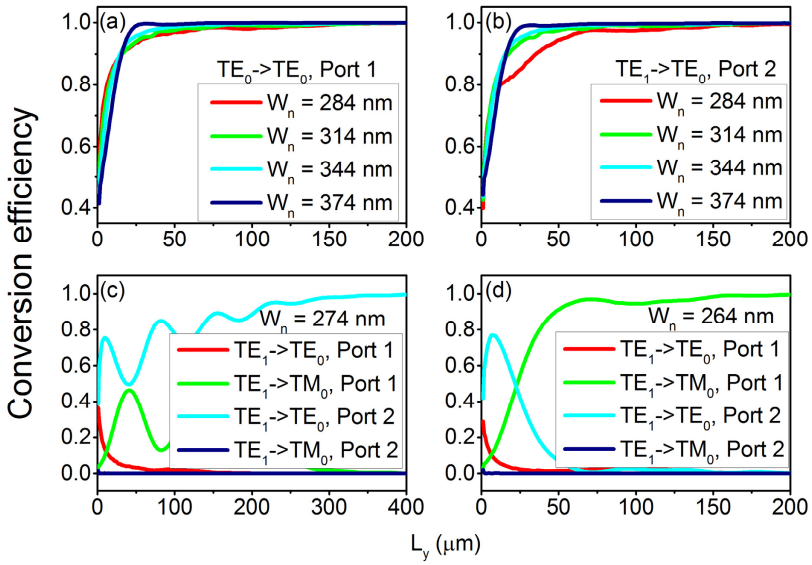

Fig. 3. The mode conversion efficiency in the asymmetric Y-junction for different input modes at the 1550 nm wavelength. (a-b) The correct mode-sorting occurs when W_n varies from 284 nm to 374 nm. (c) The undesirable mode coupling occurs when W_n = 274 nm. (d) The incorrect mode-sorting occurs when W_n = 264 nm.

Figure 4 shows the required minimum Y-junction length for various levels of mode conversion efficiency from the TE_1 mode into the TE_0 mode in port 2 as a function of W_n. Clearly there is a tradeoff between the Y-junction length and the mode conversion efficiency. By increasing the Y-junction length, improved mode conversion efficiency can be obtained in a large range for W_n, showing a potentially large fabrication tolerance compared to the DC-based PSRs. Besides, the minimum length for 99% mode conversion efficiency is achieved when W_n = 374 nm. In this case, the corresponding Y-junction length is ~30 μm.

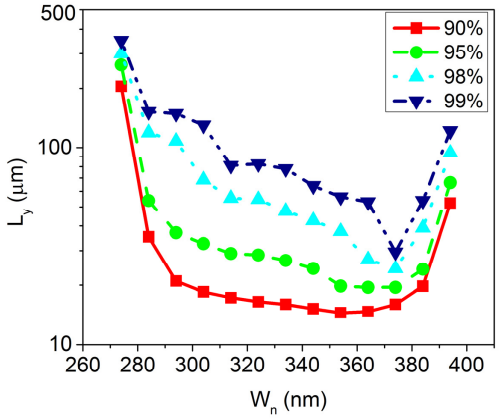

Fig. 4. The minimum Y-junction length required to achieve various levels of mode conversion efficiency from the TE_1 mode to the TE_0 mode at port 2 as a function of the narrow arm width W_n. The wavelength is 1550 nm in the simulation.

3. Device performance and fabrication tolerance analysis

Figure 5 shows the mode propagation in the PSR for different input modes at 1550 nm wavelength. According to the analysis above, the proposed PSR device has a taper length L_{tp} (= L_{tp1} + L_{tp2} + L_{tp3}) = 65 μm and a Y-junction length L_y = 30 μm, corresponding to a total

#206996 - $15.00 USD Received 10 Apr 2014; accepted 15 May 2014; published 29 May 2014
(C) 2014 OSA

length of 95 μm. The input TM_0 mode is predominantly converted into the TE_0 mode at port 2, while the input TE_0 mode is not converted in the taper and finally exits at port 1.

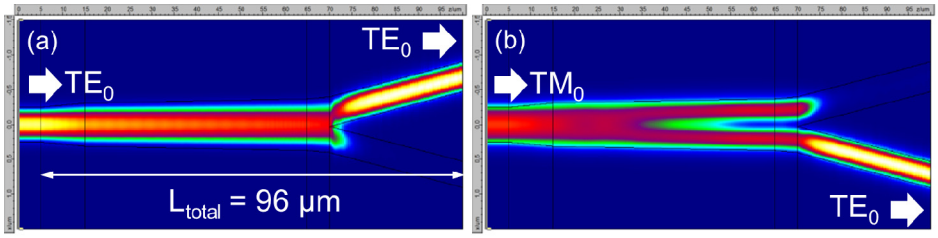

Fig. 5. Mode propagation in the device when the input is (a) the TE_0 mode and (b) the TM_0 mode, respectively. The wavelength is 1550 nm.

The wavelength dependence of the conversion efficiency at different ports is shown in Fig. 6. The simulated results were further validated by a three-dimensional finite-difference-time-domain (3D-FDTD, Lumerical FDTD) simulation and a good agreement can be seen in the figures. The optimum performance is achieved when the wavelength is ~1550 nm. Since the two basic structures in this PSR is broadband, the entire device exhibits a good performance with > 12 dB ER and < 0.4 dB IL in an ultra-broadband wavelength range from 1350 nm to 1750 nm at both ports, which significantly improved the operation bandwidth compared to all the previously reported PSRs. With such a broad operating bandwidth, this device offers potential applications for polarization diversity operating across every communication bands.

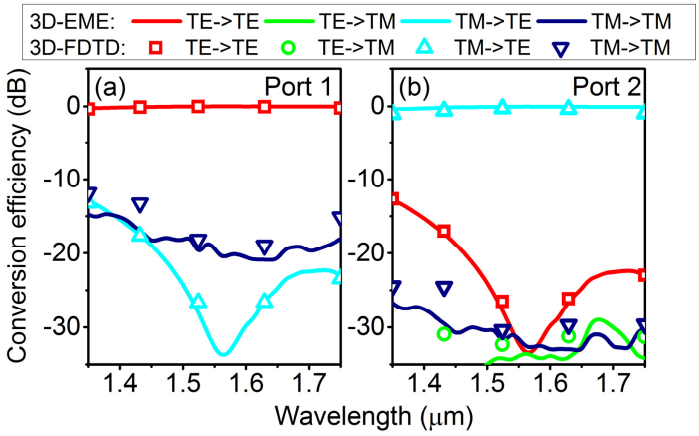

Fig. 6. The mode conversion efficiency as a function of the wavelength in the two output ports. The simulation is carried out by 3D-EME and 3D-FDTD methods. The grid size in the FDTD simulation is chosen as $\Delta x = \Delta y = \Delta z = 15$ nm. The conversion efficiency below –35 dB is not shown.

We further analyzed the performance variations due to the practical fabrication imperfections. Figures 7(a) and 7(b) show that the device has a low IL of < 0.5 dB with > 10 dB ER at both ports for the device width variation Δw from –40 nm to 70 nm and the slab height variation ΔH_{slab} from –15 nm to 15 nm. Another fabrication imperfection occurs during the upper-cladding oxide deposition, which may lead to a different refractive index of the upper-cladding from that of the bottom-cladding. Fortunately, as shown in Fig. 7(c), even though the refractive index of the upper-cladding has as high as ± 15% variation $\Delta n_{SiO2}/n_{SiO2}$ from the bottom-cladding, corresponding to n_{SiO2} changing from 1.30 to 1.76, the device performance is still very stable. We believe that these tolerances will significantly improve the manufacturing yield.

#206996 - $15.00 USD Received 10 Apr 2014; accepted 15 May 2014; published 29 May 2014
(C) 2014 OSA

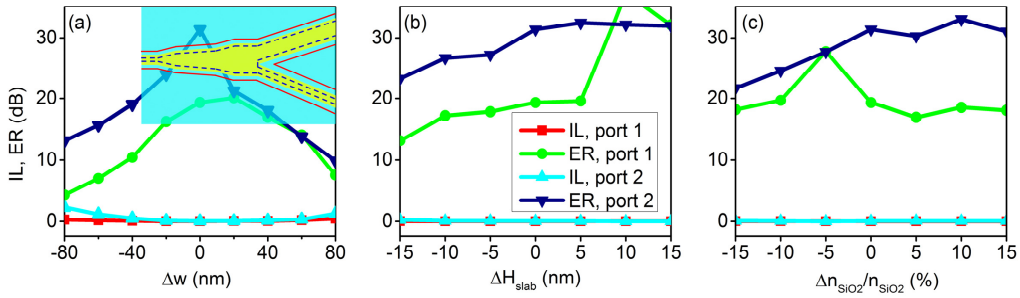

Fig. 7. Fabrication tolerance analysis for (a) the width variation Δw of the device width, (b) the variation ΔH_{slab} of the slab height, and (c) the variation of the upper-cladding refractive index. The inset of (a) shows a PSR layout affected by $\Delta w > 0$ (solid red) and $\Delta w < 0$ (dashed blue).

4. Conclusion

In summary, an ultra-broadband SOI PSR is proposed by utilizing mode-evolution tapers and a mode-sorting asymmetric Y-junction. By appropriately choosing the waveguide widths and lengths of each section in this device, high mode conversion efficiency with correct mode-sorting is obtained for the two output ports. Moreover, since the taper and Y-junction have advantages of large bandwidth and fabrication tolerance, the entire device exhibits a good performance in a large bandwidth over 400 nm as well as a large fabrication tolerance for the device width variation, the slab height variation and the imperfect upper-cladding oxide deposition.

Acknowledgments

This work was partially supported by the State High-Tech Development Plan (No. 2012AA012202), the Natural Science Foundation of Shanghai (No. 11ZR1443700) and the Natural Science Foundation of China (No. 61106051, 61107031, and 61275112). B. Niu and M. Qi were partially supported by National Science Foundation grants ECCS-0925759, CMMI-1120577, National Institute of Health grant 1R01RR026273-01 and Defense Threat Reduction Agency grant HDTRA1-10-1-0106. J. Wang acknowledges the China Scholarship Council for a student study-abroad grant. M.Q. acknowledges partial support from CAS International Collaboration and Innovation Program on High Mobility Materials Engineering.